Modeling the Size Distribution and Chemical Composition of Secondary Organic Aerosols during the Reactive Uptake of Isoprene-Derived Epoxydiols Under Low Humidity Condition

Mega Octaviani[1,†], Manish Shrivastava[1,*], Rahul A. Zaveri[1], Alla Zelenyuk[1], Yue Zhang[2,3], Quazi Z. Rasool[1], David M. Bell[4], Matthieu Riva[5], Marianne Glasius[6], Jason D. Surratt[3,7]

[1]Pacific Northwest National Laboratory, Richland, WA 99352 USA

[2]Department of Atmospheric Sciences, Texas A&M University, College Station, TX 77843 USA

[3]Department of Environmental Sciences and Engineering, Gillings School of Global Public Health, University of North Carolina at Chapel Hill, Chapel Hill, NC 27599 USA

[4]Laboratory of Atmospheric Chemistry, Paul Scherrer Institute, Villigen 5232, Switzerland

[5]Univ. Lyon, Université Claude Bernard Lyon 1, CNRS, IRCELYON, 69626, Villeurbanne, France

[6]Department of Chemistry, Aarhus University, 8000 Aarhus C, Denmark

[7]Department of Chemistry, College of Arts and Sciences, University of North Carolina at Chapel Hill, Chapel Hill, NC 27599 USA

[†]Present address: Institute of Meteorology and Climate Research, Department of Troposphere Research, Karlsruhe Institute of Technology, Karlsruhe 76021, Germany

[*]Correspondence to manishkumar.shrivastava@pnnl.gov

Submitted to ACS Earth and Space Chemistry

Keywords: secondary organic aerosols, isoprene epoxydiols, multiphase chemistry, chamber measurements, box modeling, size distribution, chemical composition, low relative humidity

Abstract

Reactive uptake of isoprene epoxydiols (IEPOX), which are isoprene oxidation products, onto acidic sulfate aerosols is recognized to be an important mechanism for the formation of isoprene-derived secondary organic aerosol (SOA). While a mechanistic understanding of IEPOX-SOA formation exists, several processes affecting their formation remain uncertain. Evaluating mechanistic IEPOX-SOA models with controlled laboratory experiments under longer atmospherically relevant timescales is critical. Here, we implement our latest understanding of IEPOX-SOA formation within a box model to simulate the measured reactive uptake of IEPOX on polydisperse ammonium bisulfate seed aerosols within an environmental Teflon chamber. The model is evaluated with single-particle measurements of size distribution, volume, density, and composition of aerosols due to IEPOX-SOA formation at timescales of hours. We find that the model can simulate the growth of particles due to IEPOX multiphase chemistry, as reflected in increases of the mean particle size and volume concentrations, and a shift of number size distribution to larger sizes. The model also predicts the observed evolution of particle number mean diameter and total volume concentrations at the end of the experiment. We show that in addition to the self-limiting effects of IEPOX-SOA coatings, accounting for the molar balance between inorganic and organic sulfate and mass accommodation coefficient of IEPOX are important parameters governing modeling of IEPOX-SOA formation. Thus, models which do not account for the molar sulfate balance and/or diffusion limitations within IEPOX-SOA coatings are likely to predict too high IEPOX-SOA formation.

Introduction

Isoprene (2-methyl-1,3-butadiene) is the non-methane volatile organic compound (VOC) emitted in largest amount to the atmosphere, with an estimated annual global emission from vegetation of 440-660 tera-grams of carbon (TgC).[1] Its abundance and rapid oxidation by

hydroxyl (OH) radicals ($k = 9.7\times10^{-11}$ cm^3 $molec^{-1}$ s^{-1})[2] plays a crucial role in tropospheric chemistry, particularly throughout forested regions in tropical and midlatitude areas. Isoprene oxidation products are significant contributors to the global budget of secondary organic aerosols (SOA),[3-5] and influence the growth and evolution of particles in ambient air, as demonstrated during laboratory experiments[6-12] and field studies[13-16] under low- and high-concentrations of nitrogen oxide ($NO_x = NO + NO_2$) conditions. On a global scale, the latest estimate of a net SOA production rate from oxidation of isoprene and other biogenic VOC is between 10-150 TgC yr^{-1}, contributing to at least 25% of total organic aerosol mass.[17, 18]

Under low-NO_x conditions, OH-initiated isoprene oxidation followed by subsequent reaction of isoprene peroxy radicals with hydroperoxyl (HO_2) radicals leads to the formation of isoprene hydroxyhydroperoxide (ISOPOOH) in yields exceeding 70%.[19, 20] ISOPOOH reacts further by OH radical addition and isomerization to form isoprene epoxydiols (IEPOX), with yields exceeding 75%.[20] Subsequent multiphase chemistry of IEPOX in the presence of aqueous, acidified sulfate aerosols has been shown to be a major source of isoprene derived SOA mass.[10, 21, 22] IEPOX uptake into the aerosol phase with further transformation via a ring-opening mechanism and nucleophilic addition in aqueous particles[22-24] explains the formation of known isoprene SOA products found in ambient aerosols, namely 2-methyltetrols, IEPOX-derived organosulfates (OSs), and oligomeric species.[10, 22, 25] Recent field measurements have demonstrated the importance of IEPOX-derived SOA products in fine organic aerosols.[26-31] In certain regions of the southeastern US, IEPOX-SOA tracers represent up to one-third of the total fine organic aerosol mass during the summer, with 2-methyltetrols and IEPOX-organosulfates contributing up to 33-47% and 15-34% of the total IEPOX-SOA, respectively.[27, 28, 31]

The reactive uptake of gas-phase IEPOX to atmospheric particles is represented by an uptake coefficient (γ_{IEPOX}). Laboratory measurements of the IEPOX uptake onto aerosol particles confirmed an increase in γ_{IEPOX} with increasing aerosol acidity.[32, 33] Furthermore, relative humidity (RH) and the presence of organic coatings also play a role in IEPOX uptake.[32, 34-37] For pure sulfate seed particles, γ_{IEPOX} exhibits an inverse correlation with RH wherein higher humidity impedes further IEPOX uptake as aerosol particles take up more water since their acidity and ionic concentrations decrease.[32, 34] Further insights into the morphology of the internally mixed organic/inorganic particles show that the presence of pre-existing SOA coatings on sulfate particles would undergo liquid-liquid or semisolid-liquid phase separation into an organic-rich shell surrounding a sulfate-containing aerosol core.[36-38] The organic shell (or coating) can suppress the acid-catalyzed heterogeneous reactions of IEPOX, as demonstrated in previous laboratory studies,[32, 34, 35] and reduce γ_{IEPOX} substantially, especially at lower RH conditions wherein OA viscosity and bulk diffusion limitations are higher.[34] In addition, IEPOX-SOA formation self-limits further IEPOX uptake. A recent study confirms that IEPOX-SOA components 2-methyltetrols and organosulfates are highly viscous and cause strong particle-phase diffusion limitations as they form a coating around the inorganic seeds during their formation.[39, 40]

Prior IEPOX-SOA modeling studies have used a resistor-based parameterization, using constraints on IEPOX solubility and reactivity, as described in Anttila et al.[41] and Gaston et al.[42] The reactivity of IEPOX is represented by an overall particle-phase reaction rate constant, where the rate-determining step depends on which of the two distinct reaction pathways, known as A-1 and A-2 mechanism, is taken.[24] Kinetic studies using bulk solutions have provided estimates of the epoxide reaction rate constants for a variety of acid-catalyzed ring-opening reactions.[24, 43-45] Several regional/global models have implemented the γ_{IEPOX} resistor-based

104 model for aqueous IEPOX-SOA formation and found improved model predictions of SOA
105 mass yield when compared to field observations.[37, 46-48]
106
107 Previous studies (e.g., Gaston et al.[32]) have measured the loss rate of IEPOX gas due to its
108 reactive uptake on acidic sulfate particles in a flow tube at short timescales (~10-20 seconds),
109 and shown that the resistor-based model can explain the IEPOX gas loss kinetics. However, to
110 the best of our knowledge, the resistor model formulation has not been tested against direct
111 measurements of particle size evolution due to IEPOX-SOA formation, especially at longer
112 timescales on the order of hours in environmental chambers. Recently, such single-particle
113 measurements have been conducted characterizing how IEPOX uptake on acidic sulfate
114 particles in a Teflon chamber affects particle size, composition and density evolution,[35]
115 providing a unique opportunity to understand IEPOX-SOA processes through application of
116 this modeling framework.
117
118 In this study, we integrated and applied new IEPOX-SOA modeling capabilities in a box model
119 to understand kinetic processes governing evolution of particle size, chemical composition, and
120 overall particle density due to reactive uptake of IEPOX, as measured by Riva et al.[35] The
121 capability of a chemistry-aerosol inorganic box model, Model for Simulating Aerosols
122 Interaction and Chemistry (MOSAIC) developed by Zaveri et al.[49], was extended to include
123 key processes of IEPOX-SOA formation on polydisperse aerosols. The MOSAIC model is also
124 widely used in regional and global chemical transport models, i.e., the Weather, Research and
125 Forecasting model with Chemistry (WRF-Chem)[50, 51] and the Community Earth System Model
126 (CESM)[52]. We then applied the model to predict the particle size evolution and SOA
127 composition upon IEPOX uptake by pure ammonium bisulfate particles from the chamber

experiments reported in Riva et al.[35] This work focuses on a single aerosol system, ammonium bisulfate seed aerosols under dry conditions (<5% RH).

Methods

MOSAIC model

In this study, we added IEPOX reactive uptake parameterizations on ammonium bisulfate (ABS) seed aerosols to the sectional aerosol box model MOSAIC (Model for Simulating Aerosol Interactions and Chemistry)[49, 53]. The model treats gas and aerosol chemistry, aerosol thermodynamics and phase state, aerosol microphysical processes such as coagulation and condensation, and particle wall loss. At every time step, it dynamically partitions nonvolatile and semi-volatile organic and inorganic gases to size-resolved particles and predicts particle-phase water and pH (acidity) in each size bin. Gas-particle mass transfer calculation takes into account compound volatility, gas-phase diffusion, interfacial accommodation, and particle-phase bulk diffusion in semisolid organic phase. For this study, particle size distribution was represented using the moving bin approach wherein coagulation was ignored, since effects of coagulation were found to be insignificant. MOSAIC was updated as described in Sections 2.3-2.6 to simulate the multi-phase chemistry, formation and time evolution of IEPOX-SOA and the resulting changes in particle size distributions and compositions within an environmental Teflon chamber.

Chamber measurements

We used the results from the experimental chamber study described by Riva et al.[35] to initialize the model with measured IEPOX gas, particle size distributions, and seed composition, and to evaluate model parameters related to IEPOX-SOA formation. Briefly, their experiments were conducted in a 1-m^3 Teflon chamber under dry (<5% RH) conditions at room temperature

(24±2°C) and atmospheric pressure (1 atm). Acidified ammonium sulfate (ammonium bisulfate, ABS) seed aerosols were generated by nebulizing aqueous solutions of 0.06 M $(NH_4)_2SO_4$ (aq) + 0.06 M H_2SO_4 (aq). The ABS seed particles were then introduced into the chamber before the injection of 500 ppb *trans*-β-IEPOX, the proposed dominant IEPOX isomer mixture.[19] *Trans*-β-IEPOX was synthesized in high purity (>99%) by the UNC group following published procedures.[54] 2.5 mg of trans-β-IEPOX was introduced into the chamber and mixed with the ABS seed particles by passing high purity N_2 gas at 2 L min^{-1} through a heated manifold (60−70 °C) for 30 min.[35] A scanning mobility particle sizer (SMPS), which consists of a differential mobility analyzer (DMA) and a condensation particle counter (CPC), was used to periodically measure the size distributions of particle number, surface area, and volume concentrations during the IEPOX uptake into the ABS seed aerosols. The single particle mass spectrometer (miniSPLAT)[55] was used to perform online in-situ measurements of size, density, shape, and chemical composition of individual particles inside the chamber at a time resolution of few minutes. A schematic of the chamber employed is shown in Fig. S1. At the end of each experiment, particles were collected onto Teflon membrane filters for offline analysis of IEPOX-derived SOA bulk chemical composition using ultra-performance liquid chromatography/electrospray ionization, high-resolution quadrupole time-of-flight mass spectrometry (UPLC/ESI-QTOFMS), and gas chromatography/electron ionization-mass spectrometry (GC/EI-MS). The experiments were also performed using deliquesced ammonium sulfate seed particles and ABS coated with SOA produced from α-pinene ozonolysis to investigate the effect of acidity and organic coating on IEPOX uptake. Further experimental details are provided in Riva et al.[35] The present study focuses on modeling IEPOX uptake onto ABS seeds under dry conditions (i.e., < 5% RH). ABS particles, even at very low

RHs, are not crystalline and instead exist in metastable states that contain some particle water,[56] which explains their high acidity and high reactivity with IEPOX under dry conditions.

IEPOX reactive uptake

The heterogeneous reactive uptake of gas-phase IEPOX on acidic seed particles is defined in terms of first-order kinetics:

$$\frac{d[\mathrm{IEPOX}_g]}{dt} = -\frac{\gamma_{\mathrm{IEPOX}}}{4} A_p \langle c \rangle [\mathrm{IEPOX}_g] \quad (1)$$

where A_p is the particle surface area (cm^2 cm^{-3}), $[\mathrm{IEPOX}_g]$ is the gas-phase IEPOX concentration (mol m^{-3}), and $\langle c \rangle$ is the mean molecular speed (cm s^{-1}). The reactive uptake coefficient of IEPOX (γ_{IEPOX}) is calculated following a resistor model described in Anttila et al.[41] that includes possible mass transfer limitations caused by organic coatings:

$$\frac{1}{\gamma_{\mathrm{IEPOX}}} = \frac{\langle c \rangle r_p}{4D_{\mathrm{gas}}} + \frac{1}{\alpha} + \frac{\langle c \rangle r_p}{4RTH_{\mathrm{org}}D_{\mathrm{org}}(q_{\mathrm{org}}F - 1)} \quad (2)$$

where D_{gas} is the gas-phase diffusion coefficient (cm^2 s^{-1}) which is estimated as $D_{\mathrm{gas}} = 1.9\mathrm{MW}^{-2/3}$ with MW being the molecular weight of IEPOX (118 g mol^{-1}), α is the mass accommodation coefficient of IEPOX (0.02 or 0.1 used here based on previous studies[32, 46, 57]), R is the ideal gas constant (L atm K^{-1} mol^{-1}), and T is the temperature (K). H_{org} and D_{org} are the Henry's law constant and diffusion coefficient of the reactant (IEPOX or 2-methyltetrols in the gas phase) in the organic coating, respectively. The terms H_{org} and D_{org} were assumed to be independent of particle size. The $H_{\mathrm{org}}D_{\mathrm{org}}$ value was determined based on SOA viscosity

199 measurements generated from a flow tube reactor conducted under a RH range of 40-99% with
200 an extrapolation for RH<40% (Fig. S2).[34] We selected the $H_{org}D_{org}$ value at 35% RH for the
201 current study (i.e., 6.34×10^{-8} M atm^{-1} cm^2 s^{-1}), as opposed to the value at the simulated dry
202 condition of <5% RH. Using extrapolated $H_{org}D_{org}$values below 35% RH completely shut off
203 reactive uptake of IEPOX (see Fig. S3) and was inconsistent with observed particle growth
204 measurements in Riva et al.[35] and other experiments at low RH.[32, 34] H_{org} was set to 2.0×10^{6}
205 M atm^{-1}, as used in Zhang et al.[34], resulting in 3.16×10^{-14} cm^2 s^{-1} for D_{org}.
206
207 The function *F* is a composite term for processes involved in the reactive uptake at the interface
208 between two bulk phases, and is expressed as:
209
210 $$F = \frac{\coth(q_{org}) + h(q_{aq}, q^*_{org})}{1 + \coth(q_{org})h(q_{aq}, q^*_{org})} \quad (3)$$

211 $$h(q_{aq}, q^*_{org})$$

212 $$= -\tanh(q^*_{org})\left[\frac{\frac{H_{aq}D_{aq}}{H_{org}D_{org}}(q_{aq}\coth(q_{aq}) - 1) - (q^*_{org}\coth(q^*_{org}) - 1)}{\frac{H_{aq}D_{aq}}{H_{org}D_{org}}(q_{aq}\coth(q_{aq}) - 1) - (q^*_{org}\tanh(q^*_{org}) - 1)}\right] \quad (4)$$

213 $$q^*_{org} = \frac{r_c}{r_p}q_{org} \quad (5)$$

214 $$q_{aq} = r_c\sqrt{\frac{k_{aq}}{D_{aq}}} \quad , \quad q_{org} = r_p\sqrt{\frac{k_{org}}{D_{org}}} \quad (6)$$

215
216 Here, H_{aq} and D_{aq} are the Henry's laws constant (3.0×10^{7} M atm^{-1}) and diffusion coefficient
217 (1.0×10^{-5} cm^2 s^{-1}) of the reactant in the inorganic aqueous core, respectively. The parameters
218 q_{aq} and q_{org} are diffuso-reactive parameters that describe the competition between diffusion

and reaction in the aqueous core and organic coating, respectively. The parameters are defined as a function of their diffusion coefficients (D_{aq} and D_{org}), radius of inorganic aqueous core (r_c) and overall particle radius ($r_p = r_c + \text{organic coating thickness}$) in cm, and the first-order reaction rate constants (k_{aq} and k_{org}) in s^{-1}. We performed a sensitivity study on model results to H_{aq} as this parameter is known to vary by several orders of magnitudes.[32, 47, 57] Fig. S4 shows that increasing H_{aq} directly contributes to an increase in SOA mass and aerosol growth, but the rate starts to slow down and the model becomes less sensitive to H_{aq} when it is higher than our default value, which is derived from measurements[44] and has been applied in past modeling studies.[28, 57-59]

The above set of equations (1-6) simulate IEPOX uptake into internally mixed organic/inorganic particles using ABS as the inorganic core and IEPOX-SOA as the organic shell. Measurements show that ABS is a highly hygroscopic substance that does not effloresce even around 0% RH and exists in a deeply metastable phase[56]. Consistent with these measurements, we assumed that ABS particles remain in a metastable liquid state at 5% RH in our MOSAIC model formulation, and its water content and acidity were approximated by not allowing the particles to effloresce.

A recent laboratory study by Zhang et al.[39] examined the implications of IEPOX-SOA on the reactivity of pre-existing sulfate particles. They found that aerosol acidity decreases, and viscosity increases after IEPOX reactive uptake, leading to a self-limiting effect where newly formed IEPOX-derived SOA inhibits additional multiphase chemical reactions of IEPOX. To account for this finding, we impose a molar balance between inorganic sulfate and

organosulfates (part of IEPOX-SOA), i.e., as organosulfate forms, an equimolar amount is lost from inorganic sulfate at each model time step.

We applied a one-second timestep to simulate the two-hour chamber experiment. The number of size bins was set to 205, with the diameters of upper and lower boundaries being 1.08 nm and 1715.45 nm, respectively. The model was initialized with gaseous IEPOX of 500 ppb and the SMPS-measured seed aerosol size distribution before the IEPOX injection. In the study, the density of 1.5 g cm^{-3} was assumed for each SOA tracer (2-methyltetrols, OSs, and oligomers), which follows an estimate applied in Cui et al.[60] It is noted that based on the miniSPLAT measurements, the density of ABS particles under dry conditions is 1.77 g cm^{-3}, while the final aerosol density after reaction with IEPOX is 1.48 g cm^{-3}. Molecular weights (MW) of 136, 216, and 250 g mol^{-1} were assigned for 2-methyltetrols, OSs, and oligomers, respectively. Oligomers of tetrols were assumed to be similar to a hemiacetal dimer of 2 IEPOX molecules, which has a MW of ~254 g $mole^{-1}$.[10, 14] The aerosol mass and number concentrations were assumed to be continuously and irreversibly lost to the walls of the Teflon chamber with a first order rate determined by fitting the measured loss in total particle number concentrations over the entire experiment (see Section S1d in the Supplement). Gas-phase wall-losses were neglected, implicitly assuming that gases deposited on the chamber walls were available to interact with particles suspended in the chamber. A sensitivity simulation where gas-phase absorption and desorption from the chamber walls was included, produced similar particle size evolution as when gas-phase wall losses were turned off (not shown).

Aqueous-phase reaction rate constant

The aqueous-phase reaction rate constant (k_{aq}) for IEPOX is calculated assuming protonation of IEPOX and nucleophilic addition following the A-2 mechanism of Eddingsaas et al.[24] We thus implemented the following definition of k_{aq}:[43, 46, 47]

$$k_{\mathrm{aq}} = \sum_{i=1}^{N} \sum_{j=1}^{M} k_{i,j} [\mathrm{acid}_i] \left[\mathrm{nuc}_j\right] \quad (8)$$

This expression implies that the overall rate of reaction is determined by the third-order rate constants ($k_{i,j}$, in M^{-2} s^{-1}) multiplied by the concentrations (mol L^{-1} within particle-phase) of acids (H^+, HSO_4^-, NH_4^+) and nucleophiles (H_2O and SO_4^{2-}) in the model. IEPOX uptake by aerosols forms two major SOA products, namely 2-methyltetrols (tetrols) and IEPOX-organosulfates (i.e., methyltetrol sulfates or OSs), based on a previous study.[61] The fraction of IEPOX-SOA attributed to OS (β) was determined based on the relative contribution of the OS formation rate to the effective first-order rate constant. The experimental values of $k_{i,j}$ were adopted from different kinetic studies compiled in Budisulistiorini et al.[46] and summarized in the Supplement (Sect. S1b and Table S1).

Tetrol phase partitioning and oligomerization

While OSs were assumed to be fully nonvolatile (consistent with the measurements of evaporation kinetics of OS standards), tetrols were treated as semivolatile which means some fraction of tetrols will partition out of the aerosols depending on the organic mass loadings. However, particle-phase tetrols were also assumed to form non-volatile oligomers at a first order timescale of ~2 hours, which reduces their evaporation/partitioning to the gas-phase, as discussed later. We assumed the saturation vapor concentration (C*) of 10 μg m^{-3} for tetrols

based on the range of C* estimates of 5-15 μg m^{-3} reported in an environmental chamber study.[61] The mass accommodation coefficient (α) of 0.1 for tetrols was applied. Diffusion limitations to the partitioning was treated based on Zaveri et al.[53], with the particle bulk diffusivity of 3.16×10^{-14} cm^2 s^{-1} (to be consistent with D_{org} parameter in Eq. 2). We also assumed that particle-phase tetrols undergo oligomerization to form non-volatile tetrol oligomers (hereinafter, referred to as oligomers) with a first order e-folding timescale (τ_{olig}) of 2 hours based on measurements reported in D'Ambro et al.[61] that the low-volatility mode of $C_5H_{12}O_4$ desorption (similar in structure to 2-methyltetrols) was formed quickly via acid-enhanced accretion chemistry within a few hours. To be consistent with the oligomerization timescale of 2 hours (7200 s), k_{org} in equation 6 was assumed to be a constant, i.e., $\frac{1}{7200}$ s^{-1}. We found that the reactive uptake coefficient of IEPOX (γ_{IEPOX}, Eq. 2) is not as sensitive to the k_{org} value except when k_{org} is very fast (10 s^{-1}) i.e. a timescale of 0.1 s (instead of 2 hours) or faster.

IEPOX-SOA processes

Fig. 1 schematically illustrates the key multiphase chemical processes during reactive uptake of IEPOX gas on aqueous acidic sulfate seed aerosols, dynamic gas-particle partitioning of tetrols and their oligomerization. After IEPOX gas dissolves in aqueous sulfate seed particles due to its high-water solubility, it undergoes acid-catalyzed particle-phase to form tetrols and OSs. Tetrols are semi-volatile and can partition back to the gas-phase, but our simulations indicate that ~50% of the tetrols are converted to non-volatile oligomers at an e-folding time scale of 2 hours. Formation of OSs consumes inorganic sulfate, decreasing particle acidity, density and hygroscopicity.[11, 35, 39] IEPOX-SOA also forms a shell around the inorganic core, and as more IEPOX-SOA forms it limits further uptake of IEPOX gases.[11] We simulated these

312 complex processes in a box model and evaluated how these processes affect size distribution,
313 chemical composition and density of the particles with respect to single-particle measurements.
314 This multi-parameter model evaluation provides unique insights and significant advances in
315 our understanding of IEPOX-SOA formation.
316
317 We further performed two sensitivity tests to examine how mass accommodation coefficient
318 and inorganic-to-organic sulfate conversion affect model performance compared to our default
319 (base case) scenario (Table 1).
320
321 **Results and discussion**
322 **Base case scenario**
323 Following IEPOX uptake and SOA formation, measurements show that the particle number
324 mean diameter increases by 52% and total suspended particle volume increases by a factor of
325 two over 2 hours, reaching final values of 127.5 nm and 42.3 μm^3 cm^{-3}, respectively (black
326 solid markers in Fig. 2). Note that actual increase in particle volume due to IEPOX-SOA
327 formation is larger if we account for particles lost to the walls of the chamber. In the base case
328 scenario, the model is able to reproduce the observed mean diameter and volume evolution,
329 but moderately underestimates their magnitudes by an average 5% and 25%, respectively (red
330 solid markers in Fig. 2). At the end of simulation, the model predicted mean diameter is 118.8
331 nm and the total volume is 32.5 μm^3 cm^{-3} (Table 1).
332
333 Fig. 3 shows evolution of particle number size distributions ($dN/dlogD_p$). The observed particle
334 size distributions are unimodal and dominated by particles in the range of 50-90 nm after 10
335 minutes and ~80-150 nm after 2 hours. The base case model well reproduces the observed
336 characteristics of unimodal structure with a shift to larger sizes as particles grow with IEPOX-

337 SOA formation. The model overestimates the initial growth of particles during the first 10
338 minutes as compared to the observations. These differences most likely relate to the fact that the
339 model was initialized "instantaneously" with gaseous IEPOX of 500 ppb and the SMPS-
340 measured seed aerosol size distribution before the IEPOX injection", whereas in the experiment,
341 it took a few minutes to inject IEPOX into 1-m^3 chamber and mix it with the ABS seed
342 particles. Fig. 2a indicates that the model reaches half of its maximum growth only within ~10
343 minutes, opposed to ~15 minutes as seen in observations[35] but reproduces the final size
344 distribution at the end of the experiment (2 hours) (Fig. 3b).
345
346 Fig. 4 shows that OSs are predicted to heavily dominate IEPOX-SOA constituents (87.4%),
347 followed by tetrols (6.0%) and tetrol oligomers (6.6%). Filter analysis by GC/EI-MS and
348 UPLC/ESI-QTOFMS reports that 2-methyltetrols and IEPOX-derived OSs contribute to
349 approximately 10% and 50-60% of IEPOX-SOA tracers, respectively (as shown in Fig. 2 of
350 Riva et al.[35]). The observations show that these species have important contributions to total
351 SOA mass (~40%), consistent with previous studies that analyzed ambient $PM_{2.5}$ samples.[22, 27]
352 C5-alkene triols are not explicitly predicted from the model, but some studies reported that
353 these could be thermal decomposition products of 2-methyltetrol-sulfates.[60, 61] As demonstrated
354 in Cui et al.[60], during GC-MS measurements, IEPOX-derived OSs can decompose into C5-
355 alkene triols (analytical GC-MS measurement artifacts) and to a smaller extent to 2-
356 methyltetrols. Therefore, the sum of measured IEPOX-OS (and their dimers/trimers) and C5-
357 alkene triols accounting for ~90% of IEPOX-SOA in Figure 2 of Riva et al. can be compared
358 to our predictions of OS. Since simulated OS represents 87% of IEPOX-SOA, these are in good
359 agreement with the sum of IEPOX-OS and C5-alkene triols in Riva et al. Given the analytical
360 artifacts involved in characterizations of IEPOX-SOA components especially through
361 techniques involving thermal decomposition, evaluating the simulated total non-volatile

content of IEPOX-SOA with observations is a key part of this puzzle. Our simulations show that the non-volatile content of IEPOX-SOA is 94% (sum of OSs and tetrol oligomers; Table 1). Complementary measurements of IEPOX-SOA evaporation kinetics at room temperature show that ~90% of IEPOX-SOA is non-volatile (Table 1). Thus, the simulated IEPOX-SOA non-volatile content agrees with measurements, which is encouraging given that particle volatility drives its lifetimes in the atmosphere.

Another important evaluation metric is total particle density, since overall density depends on particle chemical composition. The overall density of particles (organic + inorganic) measured by miniSPLAT is reported to be 1.48±0.02 g cm^{-3}.[35] Our model-predicted final particle density achieves acceptable agreement with these measurements and predicts aerosol density slightly increasing with particle size ranging between 1.50-1.65 g cm^{-3} (Fig. S6), indicating less than 12% difference between model and observations. The higher density of larger particles is due to their larger sulfate content, as governed by the polydisperse seed particle composition.

Fig. 5 shows the simulated aerosol pH, calculated as the negative logarithm of H^+ activity coefficient multiplied by H^+ mole fraction in particle liquid water. H+ activity coefficient and its mole fraction within the inorganic core are both calculated in the MOSAIC model at each timestep. The model reveals that aerosol acidity changes by more than 2 pH units from its initial value (pH = -3.43), as illustrated in Fig. 5 for a selected size bin. The rapid change in aerosol acidity after a few minutes is consistent with the declining total inorganic sulfate species (SO_4^{2-} and HSO_4^-) resulting from conversion into OSs. It has been well demonstrated that the conversion of inorganic-to-organic sulfate is driven primarily by the IEPOX to inorganic sulfate ratio (IEPOX:$Sulf_{inorg}$), with IEPOX:$Sulf_{inorg}$>10 leading to more rapid conversion of aqueous inorganic sulfate to organic components and corresponding large increase in particle

pH (lower acidity).[11, 39] Measurements in Riva et al. were conducted at an initial IEPOX:$Sulf_{inorg}$ of >20. Our simulations show that for these conditions ~80% of inorganic sulfate are converted to organo-sulfates resulting in a rapid decrease in aerosol acidity. Furthermore, OS formation also decreases aerosol hygroscopicity and diffusivity, thus limiting further IEPOX uptake.

Effect of mass accommodation coefficient

Particle growth is found to be sensitive to the mass accommodation coefficient (α) of IEPOX, a quantity describing the interfacial limitations to gaseous uptake by seed particles. It is notable that changing α from 0.02, as applied in *Base* scenario, to 0.1, as applied in *HighAccom* scenario, can increase the growth in particle number mean diameter and suspended particle volume concentration by ~8% and ~15%, respectively (Fig. 2). These results are expected, as larger values of α indicate increased gas uptake into the particle bulk. However, since α is less than unity (α=1), there still exists some barrier to mass transfer, which could be either in the condensed phase or at the particle-vapor interface. Higher α improves the model performance of predicted aerosol growth (Table 1 and Fig. 2), but the number size distribution tends to get narrower, and the peak is higher than observations (Fig. 3). Changing the α value has no discernible effect on SOA composition as shown in Fig. 4, with differences between the two scenarios are less than 3%.

Effect of accounting for molar balance between organic and inorganic sulfates

Most modeling studies do not account for sulfate balance in IEPOX-OS formation.[46, 47, 62] In our simulations above we subtracted the molar concentration of OS from inorganic sulfate at each time step, accounting for the conversion of inorganic sulfate to OS. To demonstrate the effect of this molar sulfate balance, we conducted a sensitivity study, wherein we turned off the

removal of equimolar inorganic sulfate concentrations as OS forms (*KeepSO4*). This *KeepSO4* scenario predicts a large increase in the particle number mean diameter and total volume growth, particularly after 40 mins, and overpredicts observations by ~45% and ~85%, respectively, at the end of experiment (Fig. 2). The final mean particle diameter and total volume concentration in this scenario are 189.6 nm and 79.8 μm^3 cm^{-3}, respectively (Table 1). Compared to the base case, predicted OS contribution to IEPOX-SOA within *KeepSO4* decreases by ~12% although it still dominates the SOA composition (Fig. 4). On the other hand, contribution of tetrols and its oligomers to IEPOX-SOA increase by 6% compared to the base case.

The major change in *KeepSO4* compared to the base scenario is reflected in changes of particle acidity. While in the base case pH increases by more than 2 pH units due to consumption of inorganic sulfate during OS formation, the *KeepSO4* formulation predicts a constant pH throughout the experiment as inorganic sulfate content per particle liquid water does not change (Fig. 5).

Conclusions

We derive unique insights into IEPOX-SOA processes by integrating our newly developed IEPOX-SOA formulations in a box model and unique single-particle measurements of IEPOX-derived SOA formation. While previous studies have either focused on measuring bulk kinetics, or short-timescale (~seconds) flow tube measurements of gas-phase IEPOX loss during IEPOX-SOA formation, we find that single-particle measurements within a chamber at longer timescales (~hours) and modeling of IEPOX-SOA processes provide key and valuable additional insights. We evaluate several measured parameters of IEPOX-SOA simultaneously: particle size evolution, chemical composition, density and volatility.

We find that including diffusion limitations in IEPOX-SOA organic phase and imposing an organic and inorganic sulfate molar balance are critical to explaining measured IEPOX-SOA multiphase chemistry and kinetics. Our model can simulate IEPOX-SOA formation leading to the growth of particle mean diameter and total suspended particle volume concentrations. The model also well reproduces the observed shape of the number-size distributions although it underpredicts observed aerosol mean diameter by 7% and total suspended particle volume by ~24% at the end of the experiment. However, the model overpredicts the initial growth (at t=10 min) likely because the model was initialized "instantaneously" with gaseous IEPOX of 500 ppb and the SMPS-measured seed aerosol size distribution before the IEPOX injection", whereas in the experiment, it took a few minutes to inject IEPOX into the 1-m^3 chamber and mix it with the ABS seed particles. The model reproduces the observed uniform aerosol density across particle sizes with bias of less than 12%.

The present work supports the application of IEPOX reactive uptake as an acidity-dependent SOA formation process in models and the potential impact of IEPOX-derived SOA coatings to inhibit further SOA formation. It should be noted that the model is sensitive to the mass accommodation coefficient of IEPOX, wherein a higher value of this parameter would lead to improved particle growth evolution, but the aerosol size distribution tends to be narrower, and the peak is taller than the observed data. The result entails that this parameter needs to be well constrained for accurate modeling of IEPOX-SOA. Our sensitivity study also reveals that the predicted evolution of aerosol size and volume are overestimated when inorganic sulfate is not removed during OS formation, thus highlighting the importance of accounting for the consumption of inorganic sulfate during the production of particulate OSs.

Supporting information

The Supporting information is available free of charge at http://pubs.acs.org.

Additional information on the schematic of the chamber experimental setup, particle-phase reaction rate constant (k_{aq}), selecting $H_{org}D_{org}$ and H_{aq} parameters, aerosol wall loss, comparison between simulated results and observations for the size distribution of final aerosol density, and references (PDF).

Author information

Corresponding Author

Manish Shrivastava − Atmospheric Sciences and Global Change Division, Pacific Northwest National Laboratory, Richland, Washington 99352, United States.

Email: manishkumar.shrivastava@pnnl.gov

Authors

Mega Octaviani − Atmospheric Sciences and Global Change Division, Pacific Northwest National Laboratory, Richland, Washington 99352, United States; Present address: Institute of Meteorology and Climate Research, Department of Troposphere Research, Karlsruhe Institute of Technology, Karlsruhe 76021, Germany

Rahul A. Zaveri − Atmospheric Sciences and Global Change Division, Pacific Northwest National Laboratory, Richland, Washington 99352, United States.

Alla Zelenyuk − Atmospheric Sciences and Global Change Division, Pacific Northwest National Laboratory, Richland, Washington 99352, United States.

Yue Zhang − Department of Atmospheric Sciences, Texas A&M University, College Station, Texas 77843, United States; and Department of Environmental Sciences and Engineering,

Gillings School of Global Public Health, University of North Carolina at Chapel Hill, Chapel Hill, North Carolina 27599, United States.

Quazi Z. Rasool − Atmospheric Sciences and Global Change Division, Pacific Northwest National Laboratory, Richland, Washington 99352, United States.

David M. Bell − Laboratory of Atmospheric Chemistry, Paul Scherrer Institute, Villigen 5232, Switzerland.

Matthieu Riva − Univ. Lyon, Université Claude Bernard Lyon 1, CNRS, IRCELYON, Villeurbanne 69626, France.

Marianne Glasius − Department of Chemistry, Aarhus University, 8000 Aarhus C, Denmark

Jason D. Surratt − Department of Environmental Sciences and Engineering, Gillings School of Global Public Health, University of North Carolina at Chapel Hill, Chapel Hill, North Carolina 27599, United States; and Department of Chemistry, College of Arts and Sciences, University of North Carolina at Chapel Hill, Chapel Hill, North Carolina 27599, United States.

Author contributions

M.S. designed and supervised the overall project. M.S. and M.O. implemented the IEPOX-SOA box model developments with contributions from R.A.Z., A.Z. and Y.Z. M.O. performed box model simulations and created visualizations. M.O. and M.S. wrote the Manuscript with contributions from all co-authors.

Notes

The authors declare no competing financial interests.

Acknowledgments

This research was supported by the U.S. Department of Energy (DOE) Office of Science, Office of Biological and Environmental Research. M.S., M.O. and Q.Z.R. were supported by the U.S. DOE, Office of Science, Office of Biological and Environmental Research through the Early Career Research Program. R.A.Z. and A.Z. were supported by the DOE's Atmospheric System Research Program. Pacific Northwest National Laboratory (PNNL) is operated for DOE by the Battelle Memorial Institute under contract no. DE-A05-76RLO1830. M.R. and J.D.S. wish to thank the Camille and Henry Dreyfus Postdoctoral Fellowship Program in Environmental Chemistry for their financial support. M.O received partial support for this work through the Helmholtz Association's Initiative and Networking Fund (no. VH-NG-1533). Y.Z. acknowledges the support from NSF Division of Atmospheric Geospace Sciences (AGS) grant no. 2001027 and the National Institutes of Health (NIH) training grant no. T32ES007018. The experimental studies used in this work were performed at and supported by EMSL, a DOE Office of Science User Facility sponsored by the Office of Biological and Environmental Research and located at Pacific Northwest National Laboratory. Computational resources were provided by the PNNL Institutional Computing facility and EMSL.

Tables

Table 1. Model setup and summary of observed and simulated results

Observations/ Simulation	Inorganic sulfate removal	IEPOX accommodation coefficient	Final mean diameter (nm)	Final total volume concentration ($\mu m^3\ cm^{-3}$)	IEPOX-SOA non-volatile fraction (%)
Observations			127.5	42.3	90.0
Base	ON	0.02	118.8	32.5	94.0
HighAccom	ON	0.1	128.4	37.3	93.3
KeepSO4	OFF	0.02	189.6	79.8	87.8

Figures

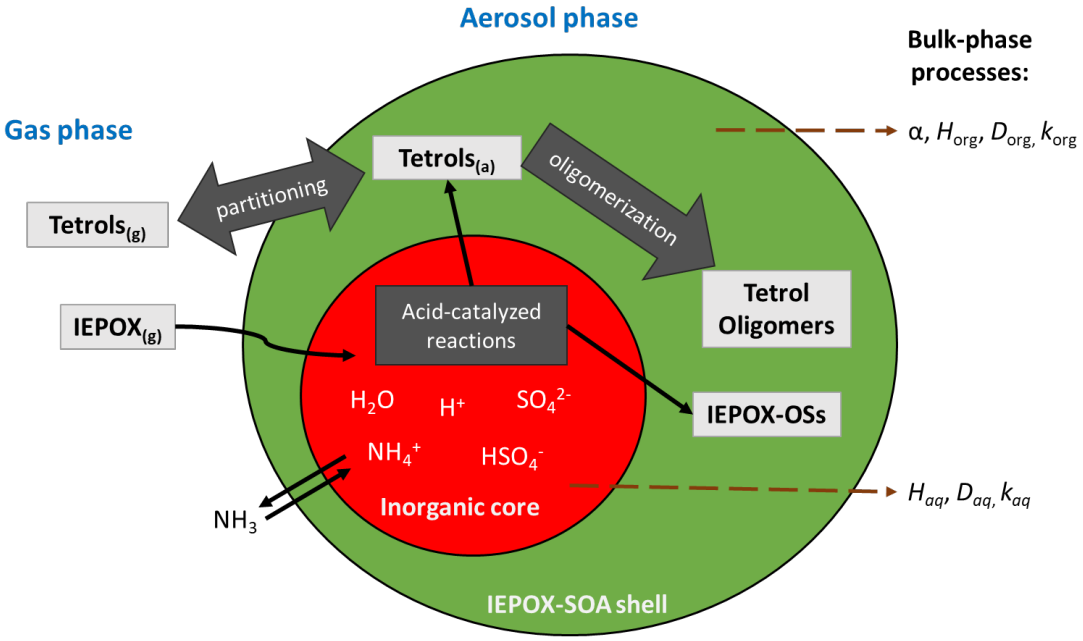

Figure 1. Schematic of IEPOX-SOA multiphase chemistry and gas-particle partitioning processes represented in the box model

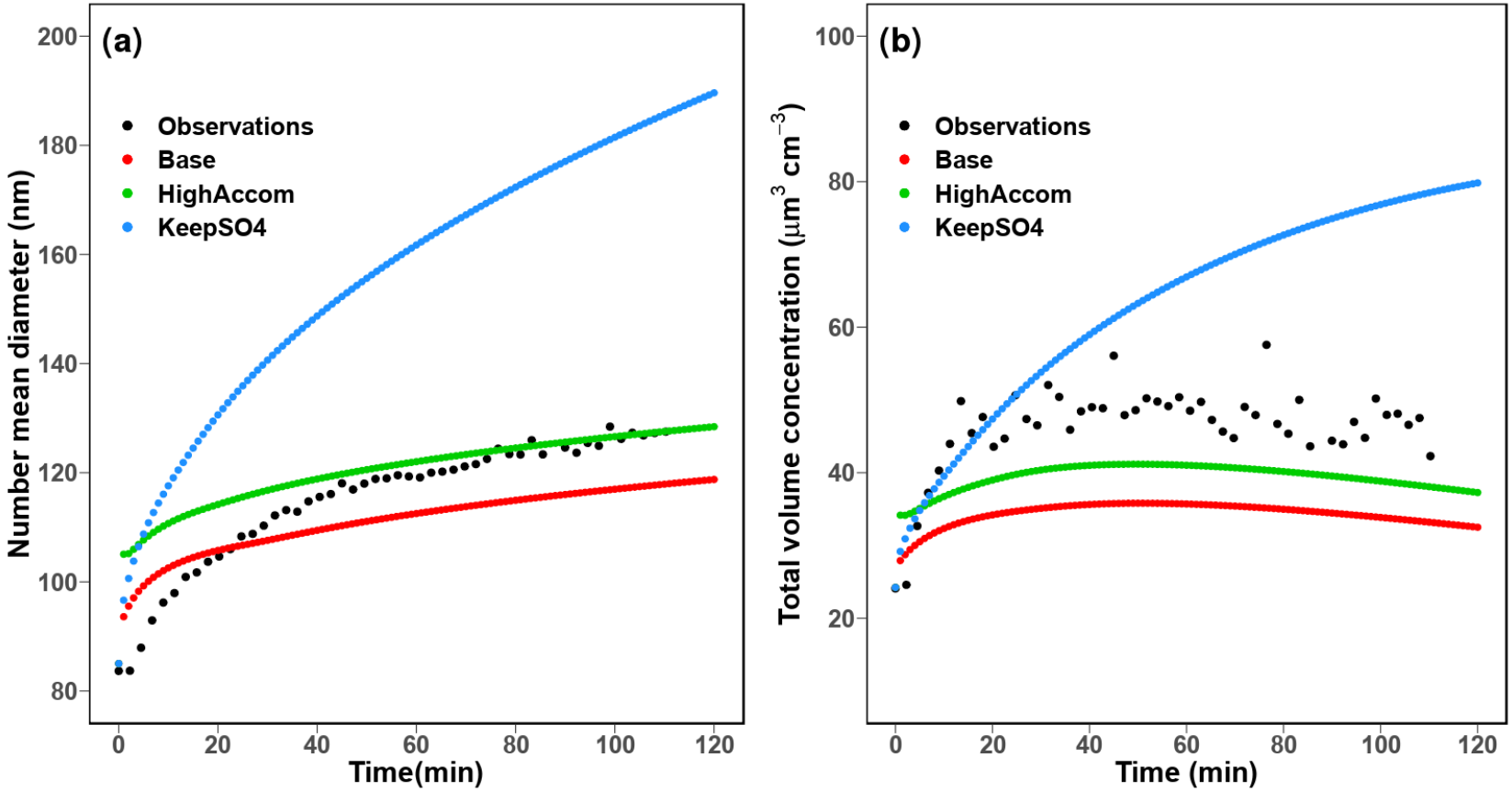

Figure 2. Time evolution of (a) aerosol number mean diameter (nm) and (b) total suspended aerosol volume concentrations ($\mu m^3\ cm^{-3}$) from observations (black dots) and all model simulations (color dots).

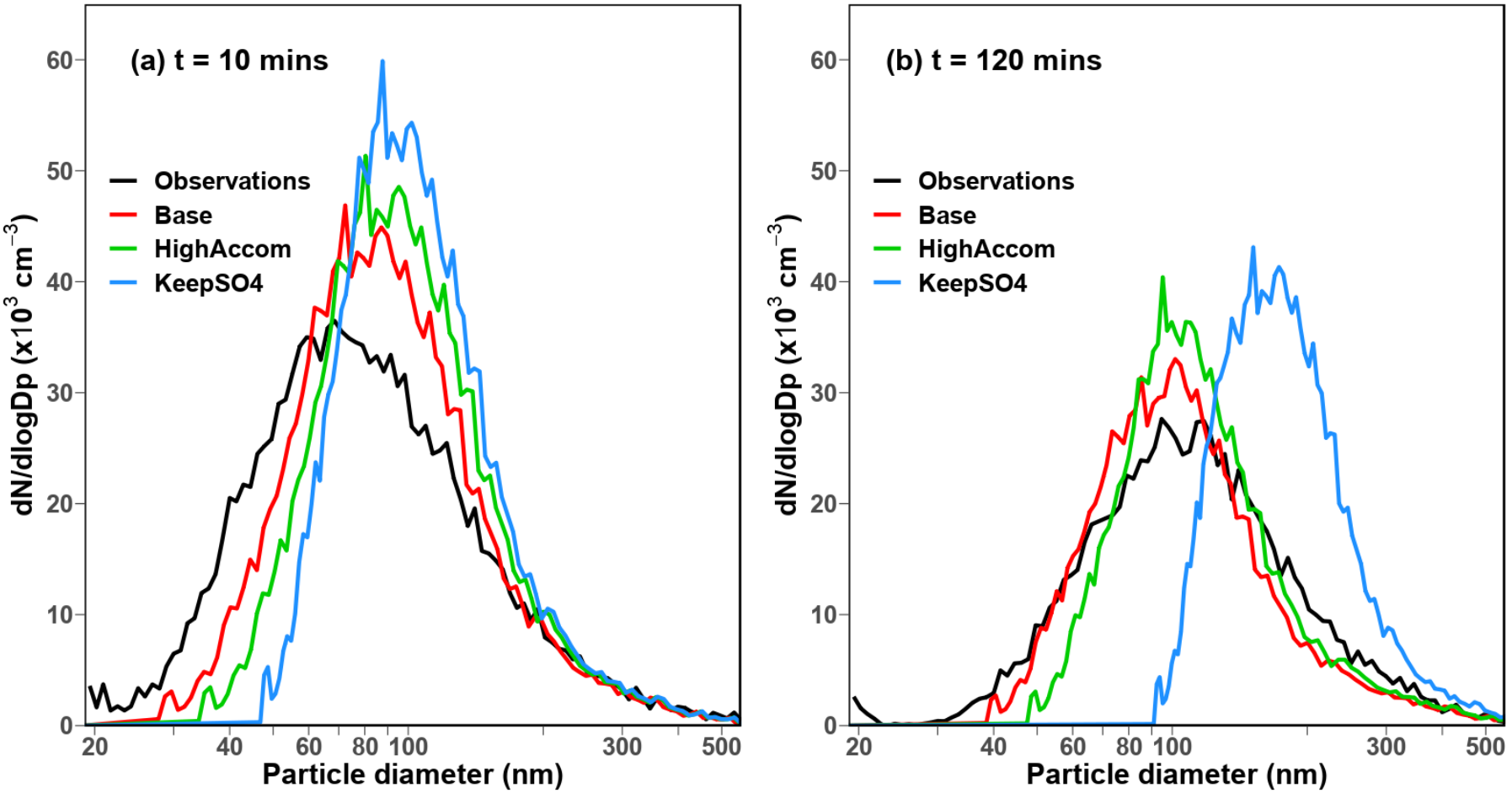

Figure 3. Size distributions of aerosol number concentrations from observations (black lines) and all model simulations (color lines) at (a) 10 and (b) 120 minutes after the introduction of IEPOX gas onto ammonium bisulfate aerosols in a 1-m^3 chamber.

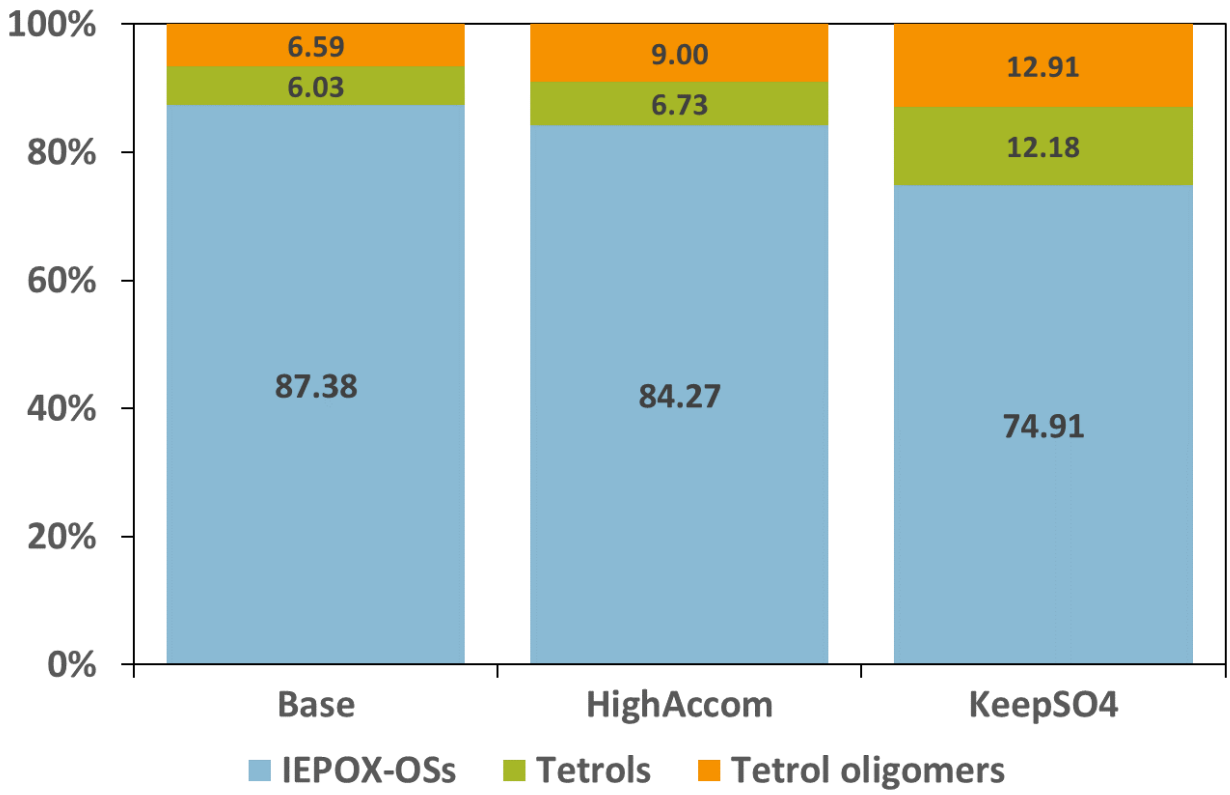

Figure 4. Relative contributions (% by mass, labels indicate the percentage values) of simulated IEPOX-derived SOA tracers for each scenario after 2 hours: IEPOX-organosulfate (OS), 2-methyltetrols (Tetrols), and tetrol oligomers.

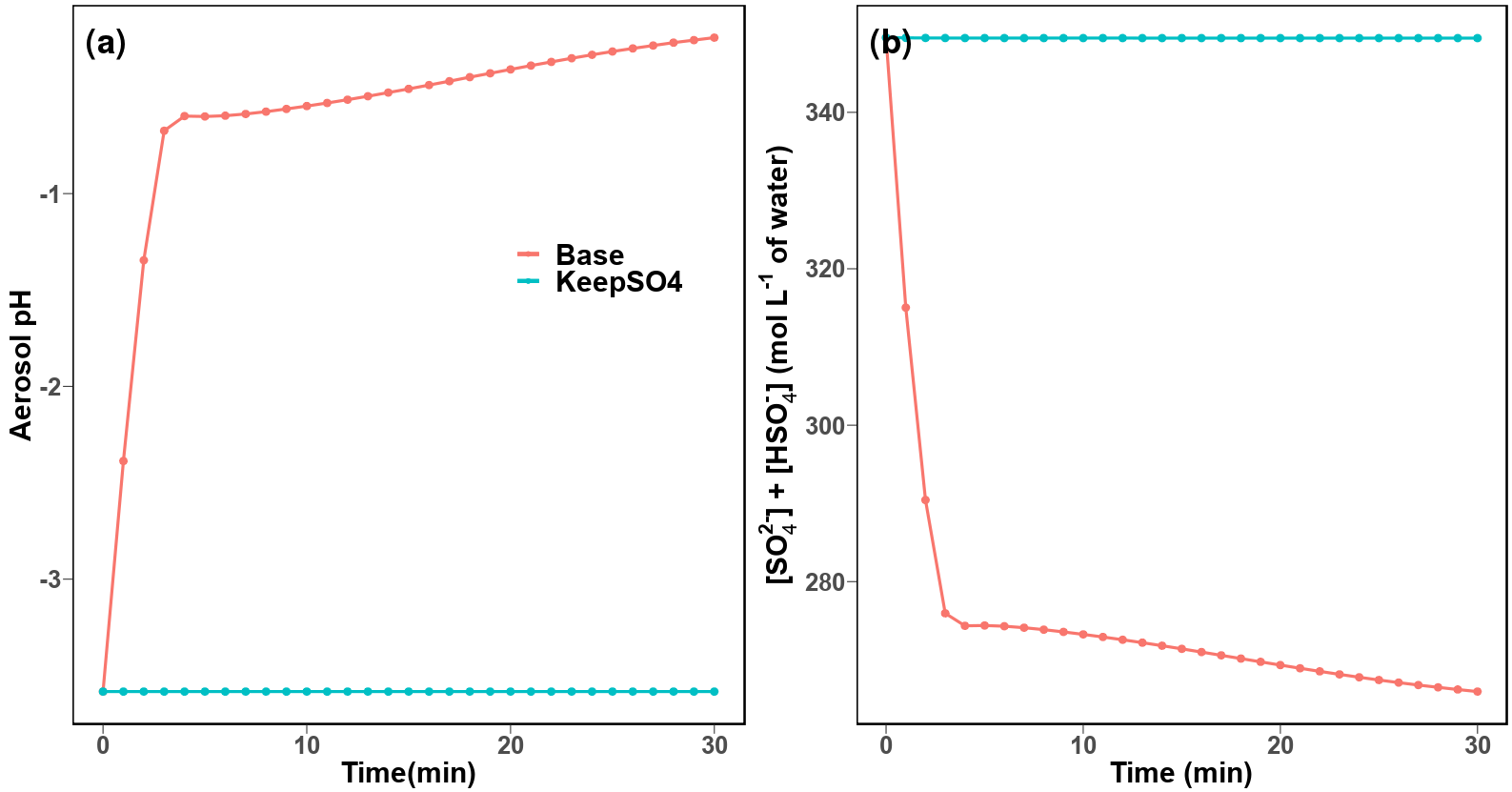

Figure 5. Time evolution of (a) simulated aerosol pH and (b) total sulfate concentration (mol L^{-1} of water) for a selected aerosol bin with the initial midpoint diameter of 85 nm.

References

1. Guenther, A.; Karl, T.; Harley, P.; Wiedinmyer, C.; Palmer, P. I.; Geron, C., Estimates of global terrestrial isoprene emissions using MEGAN (Model of Emissions of Gases and Aerosols from Nature). *Atmos. Chem. Phys.* **2006,** *6* (11), 3181-3210.
2. Atkinson, R., Gas-phase tropospheric chemistry of volatile organic compounds: 1. Alkanes and alkenes. *J. Phys. Chem. Ref. Data* **1997,** *26* (2), 215-290.
3. Carlton, A. G.; Wiedinmyer, C.; Kroll, J. H., A review of secondary organic aerosol (SOA) formation from isoprene. *Atmos. Chem. Phys.* **2009,** *9* (14), 4987-5005.
4. Henze, D. K.; Seinfeld, J. H., Global secondary organic aerosol from isoprene oxidation. *Geophys. Res. Lett.* **2006,** *33* (9).
5. Shrivastava, M.; Cappa, C. D.; Fan, J.; Goldstein, A. H.; Guenther, A. B.; Jimenez, J. L.; Kuang, C.; Laskin, A.; Martin, S. T.; Ng, N. L.; Petaja, T.; Pierce, J. R.; Rasch, P. J.; Roldin, P.; Seinfeld, J. H.; Shilling, J.; Smith, J. N.; Thornton, J. A.; Volkamer, R.; Wang, J.; Worsnop, D. R.; Zaveri, R. A.; Zelenyuk, A.; Zhang, Q., Recent advances in understanding secondary organic aerosol: Implications for global climate forcing. *Rev. Geophys.* **2017,** *55* (2), 509-559.
6. Claeys, M.; Graham, B.; Vas, G.; Wang, W.; Vermeylen, R.; Pashynska, V.; Cafmeyer, J.; Guyon, P.; Andreae, M. O.; Artaxo, P.; Maenhaut, W., Formation of secondary organic aerosols through photooxidation of isoprene. *Science* **2004,** *303* (5661), 1173-1176.
7. Edney, E. O.; Kleindienst, T. E.; Jaoui, M.; Lewandowski, M.; Offenberg, J. H.; Wang, W.; Claeys, M., Formation of 2-methyl tetrols and 2-methylglyceric acid in secondary organic aerosol from laboratory irradiated isoprene/NOX/SO2/air mixtures and their detection in ambient PM2.5 samples collected in the eastern United States. *Atmos. Environ.* **2005,** *39* (29), 5281-5289.
8. Surratt, J. D.; Murphy, S. M.; Kroll, J. H.; Ng, N. L.; Hildebrandt, L.; Sorooshian, A.; Szmigielski, R.; Vermeylen, R.; Maenhaut, W.; Claeys, M.; Flagan, R. C.; Seinfeld, J. H., Chemical composition of secondary organic aerosol formed from the photooxidation of isoprene. *J. Phys. Chem. A* **2006,** *110* (31), 9665-9690.
9. Kroll, J. H.; Ng, N. L.; Murphy, S. M.; Flagan, R. C.; Seinfeld, J. H., Secondary organic aerosol formation from isoprene photooxidation. *Environ. Sci. Technol.* **2006,** *40* (6), 1869-1877.
10. Surratt, J. D.; Chan, A. W. H.; Eddingsaas, N. C.; Chan, M.; Loza, C. L.; Kwan, A. J.; Hersey, S. P.; Flagan, R. C.; Wennberg, P. O.; Seinfeld, J. H., Reactive intermediates revealed in secondary organic aerosol formation from isoprene. *Proc. Natl. Acad. Sci. USA* **2010,** *107* (15), 6640-6645.
11. Riva, M.; Chen, Y.; Zhang, Y.; Lei, Z.; Olson, N. E.; Boyer, H. C.; Narayan, S.; Yee, L. D.; Green, H. S.; Cui, T.; Zhang, Z.; Baumann, K.; Fort, M.; Edgerton, E.; Budisulistiorini, S. H.; Rose, C. A.; Ribeiro, I. O.; e Oliveira, R. L.; dos Santos, E. O.; Machado, C. M. D.; Szopa, S.; Zhao, Y.; Alves, E. G.; de Sá, S. S.; Hu, W.; Knipping, E. M.; Shaw, S. L.; Duvoisin Junior, S.; de Souza, R. A. F.; Palm, B. B.; Jimenez, J.-L.; Glasius, M.; Goldstein, A. H.; Pye, H. O. T.; Gold, A.; Turpin, B. J.; Vizuete, W.; Martin, S. T.; Thornton, J. A.; Dutcher, C. S.; Ault, A. P.; Surratt, J. D., Increasing isoprene epoxydiol-to-inorganic sulfate aerosol ratio results in extensive conversion of inorganic sulfate to organosulfur forms: Implications for aerosol physicochemical properties. *Environ. Sci. Technol.* **2019,** *53* (15), 8682-8694.

12. Chen, Y.; Zhang, Y.; Lambe, A. T.; Xu, R.; Lei, Z.; Olson, N. E.; Zhang, Z.; Szalkowski, T.; Cui, T.; Vizuete, W.; Gold, A.; Turpin, B. J.; Ault, A. P.; Chan, M. N.; Surratt, J. D., Heterogeneous Hydroxyl Radical Oxidation of Isoprene-Epoxydiol-Derived Methyltetrol Sulfates: Plausible Formation Mechanisms of Previously Unexplained Organosulfates in Ambient Fine Aerosols. *Environ. Sci. Technol. Lett.* **2020,** *7* (7), 460-468.
13. Froyd, K. D.; Murphy, S. M.; Murphy, D. M.; de Gouw, J. A.; Eddingsaas, N. C.; Wennberg, P. O., Contribution of isoprene-derived organosulfates to free tropospheric aerosol mass. *Proc. Natl. Acad. Sci. USA* **2010,** *107* (50), 21360-21365.
14. Surratt, J. D.; Gómez-González, Y.; Chan, A. W. H.; Vermeylen, R.; Shahgholi, M.; Kleindienst, T. E.; Edney, E. O.; Offenberg, J. H.; Lewandowski, M.; Jaoui, M.; Maenhaut, W.; Claeys, M.; Flagan, R. C.; Seinfeld, J. H., Organosulfate formation in biogenic secondary organic aerosol. *J. Phys. Chem. A* **2008,** *112* (36), 8345-8378.
15. Wang, W.; Kourtchev, I.; Graham, B.; Cafmeyer, J.; Maenhaut, W.; Claeys, M., Characterization of oxygenated derivatives of isoprene related to 2-methyltetrols in Amazonian aerosols using trimethylsilylation and gas chromatography/ion trap mass spectrometry. *Rapid Commun. Mass Spectrom.* **2005,** *19* (10), 1343-1351.
16. Chan, M. N.; Surratt, J. D.; Claeys, M.; Edgerton, E. S.; Tanner, R. L.; Shaw, S. L.; Zheng, M.; Knipping, E. M.; Eddingsaas, N. C.; Wennberg, P. O.; Seinfeld, J. H., Characterization and quantification of isoprene-derived epoxydiols in ambient aerosol in the southeastern United States. *Environ. Sci. Technol.* **2010,** *44* (12), 4590-4596.
17. Hallquist, M.; Wenger, J. C.; Baltensperger, U.; Rudich, Y.; Simpson, D.; Claeys, M.; Dommen, J.; Donahue, N. M.; George, C.; Goldstein, A. H.; Hamilton, J. F.; Herrmann, H.; Hoffmann, T.; Iinuma, Y.; Jang, M.; Jenkin, M. E.; Jimenez, J. L.; Kiendler-Scharr, A.; Maenhaut, W.; McFiggans, G.; Mentel, T. F.; Monod, A.; Prévôt, A. S. H.; Seinfeld, J. H.; Surratt, J. D.; Szmigielski, R.; Wildt, J., The formation, properties and impact of secondary organic aerosol: current and emerging issues. *Atmos. Chem. Phys.* **2009,** *9* (14), 5155-5236.
18. Heald, C. L.; Henze, D. K.; Horowitz, L. W.; Feddema, J.; Lamarque, J.-F.; Guenther, A.; Hess, P. G.; Vitt, F.; Seinfeld, J. H.; Goldstein, A. H.; Fung, I., Predicted change in global secondary organic aerosol concentrations in response to future climate, emissions, and land use change. *J. Geophys. Res.: Atmos.* **2008,** *113* (D5).
19. Bates, K. H.; Crounse, J. D.; St. Clair, J. M.; Bennett, N. B.; Nguyen, T. B.; Seinfeld, J. H.; Stoltz, B. M.; Wennberg, P. O., Gas phase production and loss of isoprene epoxydiols. *J. Phys. Chem. A* **2014,** *118* (7), 1237-1246.
20. Paulot, F.; Crounse, J. D.; Kjaergaard, H. G.; Kürten, A.; St. Clair, J. M.; Seinfeld, J. H.; Wennberg, P. O., Unexpected epoxide formation in the gas-phase photooxidation of isoprene. *Science* **2009,** *325* (5941), 730.
21. Cole-Filipiak, N. C.; O'Connor, A. E.; Elrod, M. J., Kinetics of the hydrolysis of atmospherically relevant isoprene-derived hydroxy epoxides. *Environ. Sci. Technol.* **2010,** *44* (17), 6718-6723.
22. Lin, Y. H.; Zhang, Z.; Docherty, K. S.; Zhang, H.; Budisulistiorini, S. H.; Rubitschun, C. L.; Shaw, S. L.; Knipping, E. M.; Edgerton, E. S.; Kleindienst, T. E.; Gold, A.; Surratt, J. D., Isoprene epoxydiols as precursors to secondary organic aerosol formation: acid-catalyzed reactive uptake studies with authentic compounds. *Environ. Sci. Technol.* **2012,** *46* (1), 250-258.
23. Surratt, J. D.; Lewandowski, M.; Offenberg, J. H.; Jaoui, M.; Kleindienst, T. E.; Edney, E. O.; Seinfeld, J. H., Effect of acidity on secondary organic aerosol formation from isoprene. *Environ. Sci. Technol.* **2007,** *41* (15), 5363-5369.

24. Eddingsaas, N. C.; VanderVelde, D. G.; Wennberg, P. O., Kinetics and products of the acid-catalyzed ring-opening of atmospherically relevant butyl epoxy alcohols. *J. Phys. Chem. A* **2010,** *114* (31), 8106-8113.
25. Lin, Y. H.; Budisulistiorini, S. H.; Chu, K.; Siejack, R. A.; Zhang, H.; Riva, M.; Zhang, Z.; Gold, A.; Kautzman, K. E.; Surratt, J. D., Light-absorbing oligomer formation in secondary organic aerosol from reactive uptake of isoprene epoxydiols. *Environ. Sci. Technol.* **2014,** *48* (20), 12012-12021.
26. Budisulistiorini, S. H.; Canagaratna, M. R.; Croteau, P. L.; Marth, W. J.; Baumann, K.; Edgerton, E. S.; Shaw, S. L.; Knipping, E. M.; Worsnop, D. R.; Jayne, J. T.; Gold, A.; Surratt, J. D., Real-time continuous characterization of secondary organic aerosol derived from isoprene epoxydiols in downtown Atlanta, Georgia, using the aerodyne aerosol chemical speciation monitor. *Environ. Sci. Technol.* **2013,** *47* (11), 5686-5694.
27. Lin, Y. H.; Knipping, E. M.; Edgerton, E. S.; Shaw, S. L.; Surratt, J. D., Investigating the influences of SO2 and NH3 levels on isoprene-derived secondary organic aerosol formation using conditional sampling approaches. *Atmos. Chem. Phys.* **2013,** *13* (16), 8457-8470.
28. Budisulistiorini, S. H.; Li, X.; Bairai, S. T.; Renfro, J.; Liu, Y.; Liu, Y. J.; McKinney, K. A.; Martin, S. T.; McNeill, V. F.; Pye, H. O. T.; Nenes, A.; Neff, M. E.; Stone, E. A.; Mueller, S.; Knote, C.; Shaw, S. L.; Zhang, Z.; Gold, A.; Surratt, J. D., Examining the effects of anthropogenic emissions on isoprene-derived secondary organic aerosol formation during the 2013 Southern Oxidant and Aerosol Study (SOAS) at the Look Rock, Tennessee, ground site. *Atmos. Chem. Phys.* **2015,** *15* (15), 8871-8888.
29. Chen, Q.; Farmer, D. K.; Rizzo, L. V.; Pauliquevis, T.; Kuwata, M.; Karl, T. G.; Guenther, A.; Allan, J. D.; Coe, H.; Andreae, M. O.; Pöschl, U.; Jimenez, J. L.; Artaxo, P.; Martin, S. T., Submicron particle mass concentrations and sources in the Amazonian wet season (AMAZE-08). *Atmos. Chem. Phys.* **2015,** *15* (7), 3687-3701.
30. Xu, L.; Guo, H.; Boyd, C. M.; Klein, M.; Bougiatioti, A.; Cerully, K. M.; Hite, J. R.; Isaacman-VanWertz, G.; Kreisberg, N. M.; Knote, C.; Olson, K.; Koss, A.; Goldstein, A. H.; Hering, S. V.; De Gouw, J.; Baumann, K.; Lee, S. H.; Nenes, A.; Weber, R. J.; Ng, N. L., Effects of anthropogenic emissions on aerosol formation from isoprene and monoterpenes in the southeastern United States. *Proc. Natl. Acad. Sci. USA* **2015,** *112* (1), 37-42.
31. Rattanavaraha, W.; Chu, K.; Budisulistiorini, S. H.; Riva, M.; Lin, Y. H.; Edgerton, E. S.; Baumann, K.; Shaw, S. L.; Guo, H.; King, L.; Weber, R. J.; Neff, M. E.; Stone, E. A.; Offenberg, J. H.; Zhang, Z.; Gold, A.; Surratt, J. D., Assessing the impact of anthropogenic pollution on isoprene-derived secondary organic aerosol formation in PM2.5 collected from the Birmingham, Alabama, ground site during the 2013 Southern Oxidant and Aerosol Study. *Atmos. Chem. Phys.* **2016,** *16* (8), 4897-4914.
32. Gaston, C. J.; Riedel, T. P.; Zhang, Z.; Gold, A.; Surratt, J. D.; Thornton, J. A., Reactive uptake of an isoprene-derived epoxydiol to submicron aerosol particles. *Environ. Sci. Technol.* **2014,** *48* (19), 11178-11186.
33. Riedel, T. P.; Lin, Y. H.; Budisulistiorini, S. H.; Gaston, C. J.; Thornton, J. A.; Zhang, Z.; Vizuete, W.; Gold, A.; Surratt, J. D., Heterogeneous reactions of isoprene-derived epoxides: reaction probabilities and molar secondary organic aerosol yield estimates. *Environ. Sci. Technol. Lett.* **2015,** *2* (2), 38-42.
34. Zhang, Y.; Chen, Y.; Lambe, A. T.; Olson, N. E.; Lei, Z.; Craig, R. L.; Zhang, Z.; Gold, A.; Onasch, T. B.; Jayne, J. T.; Worsnop, D. R.; Gaston, C. J.; Thornton, J. A.; Vizuete, W.; Ault, A. P.; Surratt, J. D., Effect of the aerosol-phase state on secondary organic

aerosol formation from the reactive uptake of isoprene-derived epoxydiols (IEPOX). *Environ. Sci. Technol. Lett.* **2018,** *5* (3), 167-174.
35. Riva, M.; Bell, D. M.; Hansen, A.-M. K.; Drozd, G. T.; Zhang, Z.; Gold, A.; Imre, D.; Surratt, J. D.; Glasius, M.; Zelenyuk, A., Effect of organic coatings, humidity and aerosol acidity on multiphase chemistry of isoprene epoxydiols. *Environ. Sci. Technol.* **2016,** *50* (11), 5580-5588.
36. Bertram, A. K.; Martin, S. T.; Hanna, S. J.; Smith, M. L.; Bodsworth, A.; Chen, Q.; Kuwata, M.; Liu, A.; You, Y.; Zorn, S. R., Predicting the relative humidities of liquid-liquid phase separation, efflorescence, and deliquescence of mixed particles of ammonium sulfate, organic material, and water using the organic-to-sulfate mass ratio of the particle and the oxygen-to-carbon elemental ratio of the organic component. *Atmos. Chem. Phys.* **2011,** *11* (21), 10995-11006.
37. Schmedding, R.; Rasool, Q. Z.; Zhang, Y.; Pye, H. O. T.; Zhang, H.; Chen, Y.; Surratt, J. D.; Lopez-Hilfiker, F. D.; Thornton, J. A.; Goldstein, A. H.; Vizuete, W., Predicting secondary organic aerosol phase state and viscosity and its effect on multiphase chemistry in a regional-scale air quality model. *Atmos. Chem. Phys.* **2020,** *20* (13), 8201-8225.
38. Ciobanu, V. G.; Marcolli, C.; Krieger, U. K.; Weers, U.; Peter, T., Liquid–liquid phase separation in mixed organic/inorganic aerosol particles. *J. Phys. Chem. A* **2009,** *113* (41), 10966-10978.
39. Zhang, Y.; Chen, Y.; Lei, Z.; Olson, N.; Riva, M.; Koss, A. R.; Zhang, Z.; Gold, A.; Jayne, J. T.; Worsnop, D. R.; Onasch, T. B.; Kroll, J. H.; Turpin, B. J.; Ault, A. P.; Surratt, J. D., Joint impacts of acidity and viscosity on the formation of secondary organic aerosol from isoprene epoxydiols (IEPOX) in phase separated particles. *ACS Earth Space Chem.* **2019**.
40. Zhang, Y.; Nichman, L.; Spencer, P.; Jung, J. I.; Lee, A.; Heffernan, B. K.; Gold, A.; Zhang, Z.; Chen, Y.; Canagaratna, M. R.; Jayne, J. T.; Worsnop, D. R.; Onasch, T. B.; Surratt, J. D.; Chandler, D.; Davidovits, P.; Kolb, C. E., The cooling rate- and volatility-dependent glass-forming properties of organic aerosols measured by broadband dielectric spectroscopy. *Environ. Sci. Technol.* **2019**.
41. Anttila, T.; Kiendler-Scharr, A.; Tillmann, R.; Mentel, T. F., On the reactive uptake of gaseous compounds by organic-coated aqueous aerosols: theoretical analysis and application to the heterogeneous hydrolysis of N2O5. *J. Phys. Chem. A* **2006,** *110* (35), 10435-10443.
42. Gaston, C. J.; Thornton, J. A.; Ng, N. L., Reactive uptake of N2O5 to internally mixed inorganic and organic particles: The role of organic carbon oxidation state and inferred organic phase separations. *Atmos. Chem. Phys.* **2014,** *14* (11), 5693-5707.
43. Piletic, I. R.; Edney, E. O.; Bartolotti, L. J., A computational study of acid catalyzed aerosol reactions of atmospherically relevant epoxides. *Phys. Chem. Chem. Phys.* **2013,** *15* (41), 18065-18076.
44. Nguyen, T. B.; Coggon, M. M.; Bates, K. H.; Zhang, X.; Schwantes, R. H.; Schilling, K. A.; Loza, C. L.; Flagan, R. C.; Wennberg, P. O.; Seinfeld, J. H., Organic aerosol formation from the reactive uptake of isoprene epoxydiols (IEPOX) onto non-acidified inorganic seeds. *Atmos. Chem. Phys.* **2014,** *14* (7), 3497-3510.
45. Riedel, T. P.; Lin, Y. H.; Zhang, Z.; Chu, K.; Thornton, J. A.; Vizuete, W.; Gold, A.; Surratt, J. D., Constraining condensed-phase formation kinetics of secondary organic aerosol components from isoprene epoxydiols. *Atmos. Chem. Phys.* **2016,** *16* (3), 1245-1254.
46. Budisulistiorini, S. H.; Nenes, A.; Carlton, A. G.; Surratt, J. D.; McNeill, V. F.; Pye, H. O. T., Simulating aqueous-phase isoprene-epoxydiol (IEPOX) secondary organic aerosol

production during the 2013 Southern Oxidant and Aerosol Study (SOAS). *Environ. Sci. Technol.* **2017,** *51* (9), 5026-5034.
47. Pye, H. O. T.; Pinder, R. W.; Piletic, I. R.; Xie, Y.; Capps, S. L.; Lin, Y.-H.; Surratt, J. D.; Zhang, Z.; Gold, A.; Luecken, D. J.; Hutzell, W. T.; Jaoui, M.; Offenberg, J. H.; Kleindienst, T. E.; Lewandowski, M.; Edney, E. O., Epoxide pathways improve model predictions of isoprene markers and reveal key role of acidity in aerosol formation. *Environ. Sci. Technol.* **2013,** *47* (19), 11056-11064.
48. Marais, E. A.; Jacob, D. J.; Jimenez, J. L.; Campuzano-Jost, P.; Day, D. A.; Hu, W.; Krechmer, J.; Zhu, L.; Kim, P. S.; Miller, C. C.; Fisher, J. A.; Travis, K.; Yu, K.; Hanisco, T. F.; Wolfe, G. M.; Arkinson, H. L.; Pye, H. O. T.; Froyd, K. D.; Liao, J.; McNeill, V. F., Aqueous-phase mechanism for secondary organic aerosol formation from isoprene: application to the southeast United States and co-benefit of SO2 emission controls. *Atmos. Chem. Phys.* **2016,** *16* (3), 1603-1618.
49. Zaveri, R. A.; Easter, R. C.; Fast, J. D.; Peters, L. K., Model for Simulating Aerosol Interactions and Chemistry (MOSAIC). *J. Geophys. Res.: Atmos.* **2008,** *113* (D13).
50. Shrivastava, M.; Fast, J.; Easter, R.; Gustafson Jr, W. I.; Zaveri, R. A.; Jimenez, J. L.; Saide, P.; Hodzic, A., Modeling organic aerosols in a megacity: comparison of simple and complex representations of the volatility basis set approach. *Atmos. Chem. Phys.* **2011,** *11* (13), 6639-6662.
51. Shrivastava, M.; Andreae, M. O.; Artaxo, P.; Barbosa, H. M. J.; Berg, L. K.; Brito, J.; Ching, J.; Easter, R. C.; Fan, J.; Fast, J. D.; Feng, Z.; Fuentes, J. D.; Glasius, M.; Goldstein, A. H.; Alves, E. G.; Gomes, H.; Gu, D.; Guenther, A.; Jathar, S. H.; Kim, S.; Liu, Y.; Lou, S.; Martin, S. T.; McNeill, V. F.; Medeiros, A.; de Sá, S. S.; Shilling, J. E.; Springston, S. R.; Souza, R. A. F.; Thornton, J. A.; Isaacman-VanWertz, G.; Yee, L. D.; Ynoue, R.; Zaveri, R. A.; Zelenyuk, A.; Zhao, C., Urban pollution greatly enhances formation of natural aerosols over the Amazon rainforest. *Nat. Commun.* **2019,** *10* (1), 1046.
52. Zaveri, R. A.; Easter, R. C.; Singh, B.; Wang, H.; Lu, Z.; Tilmes, S.; Emmons, L. K.; Vitt, F.; Zhang, R.; Liu, X.; Ghan, S. J.; Rasch, P. J., Development and Evaluation of Chemistry-Aerosol-Climate Model CAM5-Chem-MAM7-MOSAIC: Global Atmospheric Distribution and Radiative Effects of Nitrate Aerosol. *Journal of Advances in Modeling Earth Systems* **2021,** *13* (4), e2020MS002346.
53. Zaveri, R. A.; Easter, R. C.; Shilling, J. E.; Seinfeld, J. H., Modeling kinetic partitioning of secondary organic aerosol and size distribution dynamics: representing effects of volatility, phase state, and particle-phase reaction. *Atmos. Chem. Phys.* **2014,** *14* (10), 5153-5181.
54. Zhang, Z.; Lin, Y. H.; Surratt, J. D.; Ball, L. M.; Gold, A., Technical Note: Synthesis of isoprene atmospheric oxidation products: isomeric epoxydiols and the rearrangement products cis- and trans-3-methyl-3,4-dihydroxytetrahydrofuran. *Atmos. Chem. Phys.* **2012,** *12* (18), 8529-8535.
55. Zelenyuk, A.; Imre, D.; Wilson, J.; Zhang, Z.; Wang, J.; Mueller, K., Airborne single particle mass spectrometers (SPLAT II & miniSPLAT) and new software for data visualization and analysis in a geo-spatial context. *J. Am. Soc. Mass Spectrom.* **2015,** *26* (2), 257-270.
56. Zelenyuk, A.; Cai, Y.; Chieffo, L.; Imre, D., High Precision Density Measurements of Single Particles: The Density of Metastable Phases. *Aerosol Sci. Technol.* **2005,** *39* (10), 972-986.
57. McNeill, V. F.; Woo, J. L.; Kim, D. D.; Schwier, A. N.; Wannell, N. J.; Sumner, A. J.; Barakat, J. M., Aqueous-phase secondary organic aerosol and organosulfate formation in atmospheric aerosols: a modeling study. *Environ. Sci. Technol.* **2012,** *46* (15), 8075-8081.

58. Pye, H. O. T.; Murphy, B. N.; Xu, L.; Ng, N. L.; Carlton, A. G.; Guo, H.; Weber, R.; Vasilakos, P.; Appel, K. W.; Budisulistiorini, S. H.; Surratt, J. D.; Nenes, A.; Hu, W.; Jimenez, J. L.; Isaacman-VanWertz, G.; Misztal, P. K.; Goldstein, A. H., On the implications of aerosol liquid water and phase separation for organic aerosol mass. *Atmos. Chem. Phys.* **2017,** *17* (1), 343-369.
59. Woo, J. L.; McNeill, V. F., simpleGAMMA v1.0 – a reduced model of secondary organic aerosol formation in the aqueous aerosol phase (aaSOA). *Geosci. Model Dev.* **2015,** *8* (6), 1821-1829.
60. Cui, T.; Zeng, Z.; dos Santos, E. O.; Zhang, Z.; Chen, Y.; Zhang, Y.; Rose, C. A.; Budisulistiorini, S. H.; Collins, L. B.; Bodnar, W. M.; de Souza, R. A. F.; Martin, S. T.; Machado, C. M. D.; Turpin, B. J.; Gold, A.; Ault, A. P.; Surratt, J. D., Development of a hydrophilic interaction liquid chromatography (HILIC) method for the chemical characterization of water-soluble isoprene epoxydiol (IEPOX)-derived secondary organic aerosol. *Environ. Sci.: Processes Impacts* **2018,** *20* (11), 1524-1536.
61. D'Ambro, E. L.; Schobesberger, S.; Gaston, C. J.; Lopez-Hilfiker, F. D.; Lee, B. H.; Liu, J.; Zelenyuk, A.; Bell, D.; Cappa, C. D.; Helgestad, T.; Li, Z.; Guenther, A.; Wang, J.; Wise, M.; Caylor, R.; Surratt, J. D.; Riedel, T.; Hyttinen, N.; Salo, V. T.; Hasan, G.; Kurtén, T.; Shilling, J. E.; Thornton, J. A., Chamber-based insights into the factors controlling epoxydiol (IEPOX) secondary organic aerosol (SOA) yield, composition, and volatility. *Atmos. Chem. Phys.* **2019,** *19* (17), 11253-11265.
62. Schmedding, R.; Ma, M.; Zhang, Y.; Farrell, S.; Pye, H. O. T.; Chen, Y.; Wang, C.-t.; Rasool, Q. Z.; Budisulistiorini, S. H.; Ault, A. P.; Surratt, J. D.; Vizuete, W., α-Pinene-Derived organic coatings on acidic sulfate aerosol impacts secondary organic aerosol formation from isoprene in a box model. *Atmos. Environ.* **2019,** *213*, 456-462.

TOC Figure

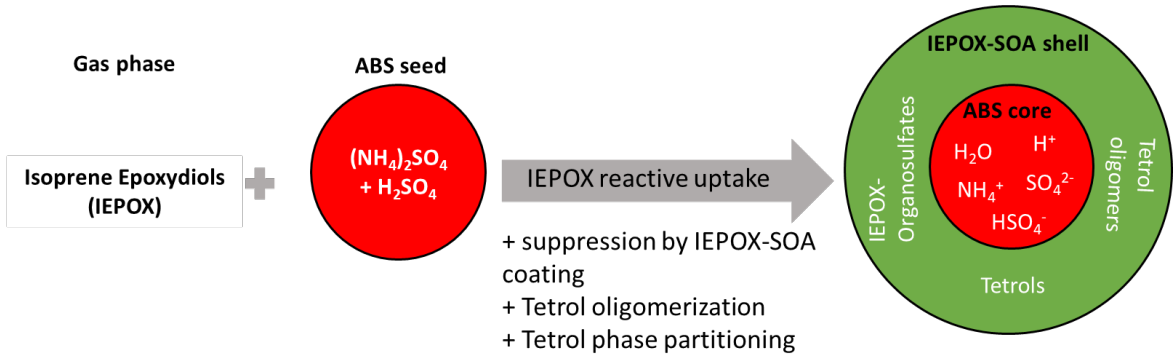
Gas phase
ABS seed
Isoprene Epoxydiols (IEPOX)
$(NH_4)_2SO_4$ + H_2SO_4
IEPOX reactive uptake
+ suppression by IEPOX-SOA coating
+ Tetrol oligomerization
+ Tetrol phase partitioning
IEPOX-SOA shell
ABS core
H_2O
H^+
NH_4^+
SO_4^{2-}
HSO_4^-
IEPOX-Organosulfates
Tetrol oligomers
Tetrols